Contents lists available at ScienceDirect

Chemical Physics Letters

Facet enhanced photocatalytic effect with uniform single-crystalline zinc oxide nanodisks

Jing Hui Zeng [a,b,c,*], Bin Bin Jin [a], Ye Feng Wang [a,c]

[a] School of Chemistry and Materials Science, Shaanxi Normal University, Xi'an 710062, China
[b] Key Laboratory of Macromolecular Science of Shaanxi Province, Shaanxi Normal University, Xi'an 710062, China
[c] NanoGen Co. Ltd., Hefei 230026, China

ARTICLE INFO

ABSTRACT

Uniform single-crystalline ZnO nanodisks and nanowires (thick and thin nanowires) with well-developed facets have been synthesized hydrothermally. It is demonstrated that the unique ZnO nanodisks with a high (0001) facet population and small surface area show the best photocatalytic activity among the samples. All the samples are in the same comparable dimension and surface area regime and the design of nanodisk and nanowire reduce the effect of unwanted facet effect to a degree as minimum as possible when catalytic activity of (0001) and $\{10\bar{1}0\}$ facets are compared. The results indicate that photocatalytic activity strongly depend on specific crystal planes.

1. Introduction

Single-crystalline nanoparticles with designed facet, which show enhanced catalytic reactivity, attract much research interest recently [1–6]. For example, microcrystalline MgO {100} face is particularly important in appropriate adsorption, molecular trafficking, and desorption [2]. Pt {111} facets show much better methanol oxidation reactivity in fuel cell tests [3]. Tetrahexahedral platinum nanocrystals behaves high electro-oxidation activity [1a]. Anatase single crystals with large percentage {001} facet for especially high catalytic reactivity [1b]. Besides, catalysts with certain selected facet may be served as asymmetric catalyst in organic reactions for chiral products [4]. Both theoretic calculations and experimental data are collected to illustrate the facet related catalytic activities [5,6]. The urgency is also reflected and highlighted in the synthesis art of single-crystalline nanoparticles of high active nanocatalysts with selected crystal faces [7].

The photocatalyzed degenerations of water or air pollutants are one important application of catalytic reactions due to the requirements of sustained developments [8]. Semiconductor metal oxide (and sulfide) catalysts, such as TiO_2, ZnO, CdS, WO_3, etc. have attracted much attention. Among these catalysts, ZnO, a direct wide band gap (3.37 eV) semiconductor, is of great importance. For example, sulfur-containing molecules are removed from the feed-stream by adsorption on a bed of ZnO [9]. Zinc oxide is able to catalyze the reduction of nitrogen dioxide by alkanes [10]. French et al. formulate a catalytic cycle for the hydrogenation of CO_2 to methanol in a synthesis gas mixture containing CO_2 and H_2 recently [11]. ZnO catalyzes the generation of hydrogen peroxide effectively under UV irradiation [12]. Hydrogen peroxide can be utilized for the degradation of organic pollutants and sterilize bacteria and viruses [12,13]. These ZnO catalyzed reactions can be conducted in nearly neutral solution, which is another advantage of ZnO over its competitors and makes ZnO a significant candidate for environmental protection.

Due to the desired chemo-physical properties related to definite facet, size and morphology controlled syntheses of ZnO nanostructures have been studied. Nanowires [14], nanoplates [15,16], nanobelts [17], nanorods [18], nanotubes [19], nanonails [20], and hierarchical nanostructures composed of rod-like and plate-like components [21], etc. were prepared using different synthetic strategies including vapor phase, sonochemical, and wet-chemical reactions [18,22]. Catalytic behaviors were also evaluated using some of these nanostructures [23], especially for nanoplates [12], nanorods, nanowires [24], and their complecting structures [25]. The high catalytic activities are attributed to the large specific surface area [22,23], and well-defined crystal planes from or single crystals [26] or nanocrystallines [24,25,27].

Anyway, there still exists arguing on comparing the catalytic activities using nanocrystallines with well-defined facet yet in comparable dimension, surface area, and crystallinity. The synthesis of uniform single-crystalline ZnO nanostructures, especially round nanodisks, thus remains a major draw back to this point. Although ZnO hexagonal nanoplates with high (0001) facet population have been synthesized, many other parameters interfere the comparison of the catalytic behavior between the high population (0001) facet of plates with $\{10\bar{1}0\}$ facets of nanowries. For example, to bring a comparable surface area of nanoplates and nanowires into the same

---

* Corresponding author. Address: School of Chemistry and Materials Science, Shaanxi Normal University, Xi'an 710062, China. Fax: +86 29 8530 7774.
   E-mail address: nanosci@snnu.edu.cn (J.H. Zeng).

scale, thin plates with large plate dimensions and wires with relative large diameter is a prerequisite. If the plates grow too thick and the thickness is in the same regime of the plates' dimension, plates develop into prisms. As a result, the catalytic effect of $\{10\bar{1}0\}$ facets surrounding the plates cannot be totally excluded. Even in the thin plate case, the dimensional effect, which reduces the charge carrier recombination and enhances the catalytic effect, cannot be fully ruled out, which means the catalytic activity is not contributed only by the facet effect. So the synthesis of single-crystalline nanodisks with comparable dimension with that of nanowires for the comparison of facet related catalytic behavior remains a challenge. Compared with hexagonal plates, even with thick plates, the suppression of characteristic $\{10\bar{1}0\}$ facets perpendicular to (0001) facet of the nanodisks will reduce the effect other than (0001) facet to the minimum during the comparison of photocatalytic activities, which is another advancement for the synthesis of the unique single-crystalline ZnO nanodisks. The present work bridges the fundamental studies in surface science and practical applications in, for example, catalyst, photovoltaic cells, sensors, and so on.

In this Letter, uniform single-crystalline ZnO nanodisks and nanowires with well-defined facets have been synthesized hydrothermally. ZnO nanodisks with high (0001) population show superior photocatalytic reactivity to that of nanowires despite of nanodisk's smaller surface area.

2. Experimental

All reagents, including zinc acetate dihydrate ($Zn(OAc)_2 \cdot 2H_2O$), sodium hydroxide (NaOH), sodium citrate, Rhodamine B (RhB) and absolute ethanol, were analytical grade, purchased from Xi'an Chemical Industrial Co., and used without further purification.

Synthesis of the ZnO nanodisks and nanowires. Zinc acetate dihydrate (0.55 g) and 0.74 g of sodium citrate were dissolved in 40.0 mL deionized water. After the salts were dissolved, 4.0 mL of 1–4 M sodium hydroxide solution was added to the solution under continuous stirring for 1 h. The final mixture was transferred to a 50 mL Teflon-lined stainless steel autoclave for hydrothermal reaction at 120 °C in an oven for 8 h. When the reaction was completed, the autoclave was cooled to room temperature naturally. The resulting white precipitate was collected by centrifugation and purified by washing with deionized water and absolute ethanol several times, and finally dried at 60 °C for 8 h.

For the synthesis of nanowires, 0.11 g of zinc acetate dihydrate and 0.53 g of sodium citrate were dissolved in 25.0 mL of deionized water to form a clear solution. Ten milliliter of 1–3 M sodium hydroxide solution was then added to the above solution under continuous stirring for 30 min. After that, the solution was hydrothermal treated at 200 °C for 12 h to carry out the reaction. The treatments of products were the same as that for ZnO nanodisks.

Controlled experiments were conducted to study the formation mechanism of ZnO nanodisks and nanowires with different concentrations of raw materials along with varying reaction temperature and time from 120 to 200 °C and 8–12 h, respectively. The detailed experimental parameters had been discussed for the different ZnO formation mechanism in our works [28].

Measurement of photocatalytic property. The photocatalytic activity of ZnO nanodisks and nanowires were evaluated by measuring the photodegradation efficiency of RhB aqueous solution under the illumination of UV. In the photocatalytic activity experiments, a cylindrical pyrex flask (100 mL) was used as the photoreactor vessel. Thirty watts UV lamps (Philips) with 254 nm irradiation were employed as the light source. The light intensity was $6.0 \times 10^3 \,\mu W/cm^2$. The sample (0.06 g) and 60 mL of 1.25×10^{-5} mol/L RhB solution were mixed by magnetic stirrer for 1 h in dark to keep the reactive system uniform and to ensure the adsorption/desorption equilibrium of dyes with the ZnO powder. Then, the UV lamps were turned on to begin illuminating. The solution was sampled in 2 h intervals. The photodegradation efficiency was monitored by measuring the absorbance of the solution samples at its maximum absorption wavelength of 553 nm with a UV–vis spectrophotometer (TU-1901, Purkinje General Co.) at room temperature.

Characterization. The phase and purity of the ZnO nanostructures were characterized by powder X-ray diffraction (XRD), using a Rigaku (Japan) D/Max2550VB+/PC X-ray diffractometer equipped with Cu Kα radiation (λ = 1.5418 Å) at a scanning rate of 8°/min for 2θ ranging from 20° to 70°. The operation voltage and current were 40 kV and 40 mA, respectively. The size and morphology were observed using Philips-FEI Quanta 200 scanning electron microscope (SEM) with an operation voltage of 20 kV. High-resolution electron microscopy (HRTEM) images were taken on a JEOL JEM-2010 high resolution transmission electron microscopy. The BET surface area of catalysts was measured by N_2 adsorption using a specific surface area analyzer (SA-3100, Beckman Coulter Co.). Fourier transform infrared (FT-IR) spectra were collected on a Brucker EQUINX55 spectrometer.

3. Results and discussion

Structure and morphology. The morphology and size of the ZnO nanostructures were initially examined by SEM. Fig. 1a and b shows SEM images of the unique ZnO nanodisks. The nanodisks, like small troches, are dominated by circular columned-based thin disks with uniform size and well-defined shape. The disks are about 1.5 μm in diameter and 300 nm in thickness. Fig. 1c–f reveals that the nanowires are dominated by well-faceted hexagonal columns. The average diameter of thick ZnO nanowires (Fig. 1c and d) is about 750 nm with about 80 μm in length (aspect ratio (l/d) > 100:1), while the average diameter of thin ZnO nanowires (Fig. 1e and f) is about 200 nm with a length of about 100 μm (aspect ratio (l/d) > 450:1). Furthermore, the nanowires have very sharp tips, pointing like a sword or pyramid (inset in Fig. 1d and f).

Further structural characterizations on the faceted ZnO nanocrystllines are performed using HRTEM. Fig. 2 shows the HRTEM images of the ZnO nanodisks and nanowires. The HRTEM images indicate that both nanodisks and nanowires are single crystalline. Moreover, there does not appear to be any significant amorphous ZnO or defects on the exterior of the nanodisks and nanowires. Fig. 2a is a HRTEM image of a nanodisk viewing from [0001] zone axis. The lattice spacing is 0.28 nm, which corresponds to that of $(10\bar{1}0)$ planes. This indicates that the nanodisk grows mainly perpendicular to [0001] zone axis, and the growth along $\langle0001\rangle$ direction is suppressed. Fig. 2b indicates the growth along $\langle0001\rangle$ direction and the formation of nanowires. The lattice spacing (0.26 nm) corresponds to the distance between two (0001) planes. Each individual ZnO nanowire is a perfect single crystalline with its c axis as the growing direction. The preferred growth along $\langle0001\rangle$ direction of nanowires is also later reflected in the XRD patterns. SEM and HRTEM analysis clearly demonstrate that the predominantly exposed planes of nanodisks are {0001} planes and the well-faceted nanowires have a larger population of $(01\bar{1}0)$ planes. Fig. 3 gives a schematic illustration of the growth models for the nanodisks and nanowires.

Phase purity is characterized by power X-ray diffractions. Fig. 4 shows typical XRD patterns of nanodisks and nanowires. All the reflection peaks of three nanostructures can be readily indexed to pure ZnO with wurtzite structure (JCPDS No. 36-1451, space group P63mc (186)). The calculated lattice constants are a_A = 3.2563 Å, c_A = 5.1980 Å; a_B = 3.2678 Å, c_B = 5.2221 Å and a_B = 3.2553 Å, c_B = 5.2139 Å for ZnO nanodisks, thick nanowires and
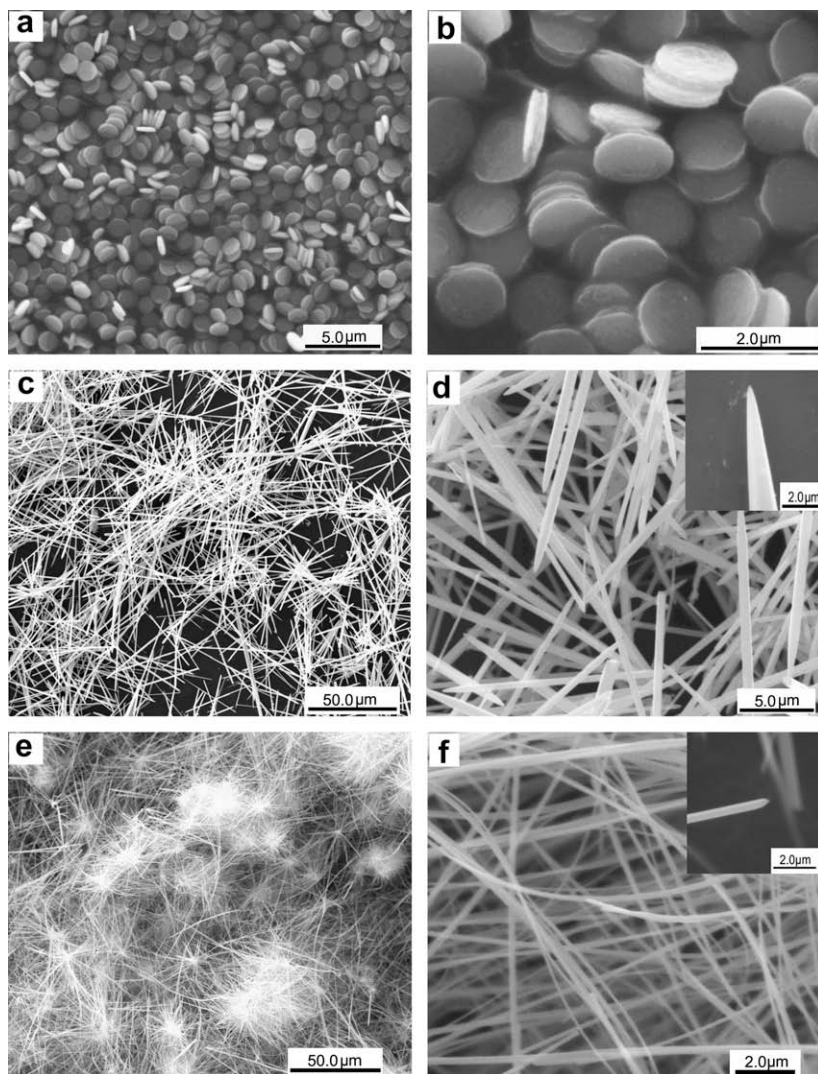
Fig. 1. SEM images of the uniform ZnO nanostructures (a) and (b) nanodisks of about 1.5 μm in diameter and 300 nm in thickness; (c) and (d) thick nanowires of 750 nm in diameter and (e) and (f) thin nanowires of 200 nm in diameter. The nanowires are with sharp tips (insert d and f).

thin nanowires, respectively. Three lattice parameters are in good agreement with those in the JCPDS card. We can also notice that the patterns (Fig. 4b and c) show suppressed (hkl) reflections $(l \neq 0)$. The weak (hkl) peaks $(l \neq 0)$ suggest that the dominate

morphology of as-prepared ZnO is wire-shaped with a preferential orientation along $\langle 0001 \rangle$ and these nanowires mainly lie on the surface of the sample grid during XRD characterizations. The phenomena are in good coincident with those observed with SEM and
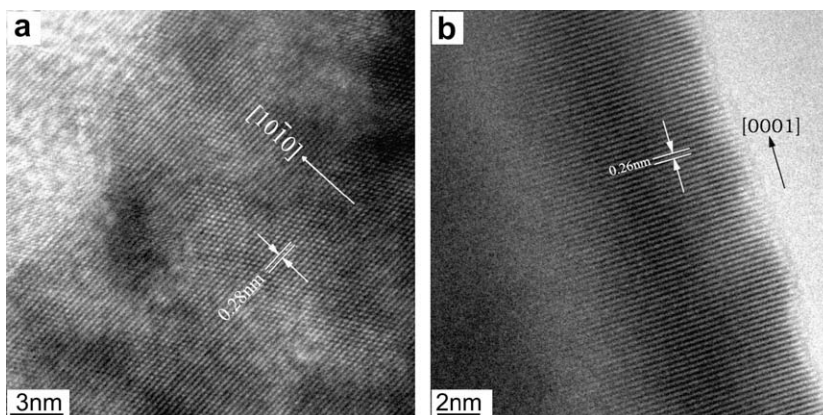

Fig. 2. Lattice fringe images of single-crystalline ZnO nanostructures. (a) ZnO nanodisks show a growth perpendicular to [0001] zone axis, (b) ZnO nanowires growing along $\langle 0001 \rangle$ direction.
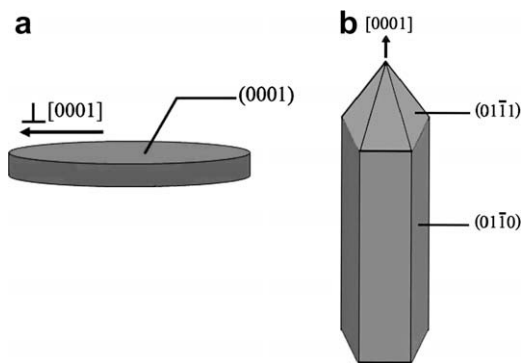
Fig. 3. Schematic illustration of the growth models for (a) nanodisks and (b) nanowires.

Fig. 5. FT-IR spectra of ZnO with different morphologies. (a) nanodisks, (b) thin nanowires, (c) thick nanowires. The absence of carbonyl peak around 1730 cm^{-1} indicates removing of citrate during the washing process.
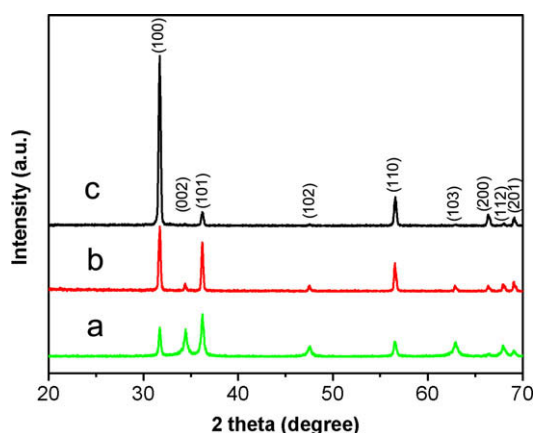

Fig. 4. Powder XRD patterns of ZnO nanostructures (a) nanodisks; (b) thick nanowires and (c) thin nanowires.

HRTEM. For the nanodisks, they tend to set randomly on the sample grid during XRD test, so there is no obvious XRD peak suppression owning to both preferred growth and sample orientation during XRD characterization.

Photocatalytic differentiation of ZnO nanodtructrues. The largest obstacles for the comparison of nanocrystallines are the compatible surface chemistry and shape retention [7c]. We have synthesized nanodisks and nanowires with well-defined facet, by which the first obstacle is cleared. The second problem is mainly related to the surfactant and other morphology controlling reagents capping on the surface of nanocrystallines, which is used during the synthesis procedure. Removing the reagents always results in significant morphology change via surface reconstruction, particle ripening, melting, or oxidation. However, due to the relative large crystalline dimension, after removing surfactant, sodium citrate, the size and morphology does not manifest observable change as observed in crystals in dimensions of hundred nanometer scale [1].

The removing of capping agents is confirmed by the absence of characteristic peaks of citrate on different ZnO nanostructures in FT-IR spectra (Fig. 5). The FT-IR spectra of both nanodisks (Fig. 5a) and nanowires (Fig. 5b and c) show main absorption bands at 3400–3500 cm^{-1}, 2900–3000 cm^{-1}, 1380–1400 and 1600–1650 cm^{-1}, which correspond to the O–H mode, C–H mode, and asymmetric and symmetric C=O stretching modes of zinc acetate, respectively. The absorption band at 470–530 cm^{-1} is the stretching mode of ZnO [29]. A distinct carbonyl peak around 1730 cm^{-1} in citrate is absent for all the samples, which indicates that citrate was fully removed during the washing process [30]. By the removal
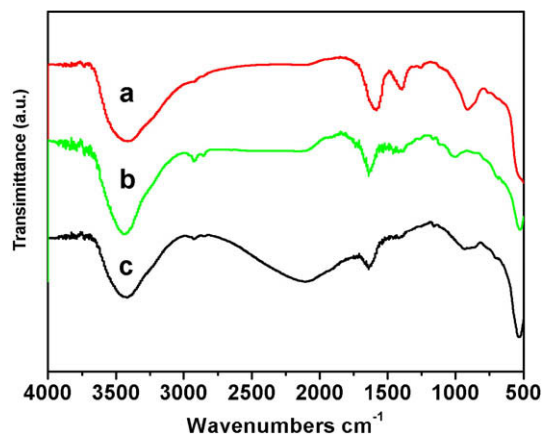
of the capping agents, the catalytic active sites of ZnO nanodisks and nanowires are accessible.

To evaluate the photocatalytic activity of ZnO nanostructures, Rhodamine B (RhB) solution has been chosen as a model compound [31]. With the uniform single-crystalline ZnO nanodisk and nanowires, we were able to clearly investigate the photocatalytic activity by monitoring the UV–vis spectra of RhB solution when the dye is photocatalytic degradated by the as-prepared ZnO nanodisks and nanowires (Fig. 6). Under UV-light irradiation, but in the absence of any catalysts, the concentration of Rhodamine B changed little after irradiation (Fig. 6d). The result indicated that the photoinduced self-sensitized photolysis of Rhodamine B can be neglected. However, with the addition of any catalysts, the photodegradation was distinctly enhanced. We can clearly observed the absorption peaks of RhB aqueous solutions in the presence of ZnO nanodisks (Fig. 6a), thick nanowires (Fig. 6b) and thin nanowires (Fig. 6c) diminished gradually with the increasing exposure time. The constant decreasing of absorbance was attributed to the destruction of the chromogen in RhB. There was no new absorption peak appeared so that the monitoring of photocatalytic activity was not affected by other factors. The photodegradation of RhB catalyzed by the ZnO nanostructures fits pseudo first-order reaction well, i.e., $-dc/dt = Kt$, or $\ln(C_0/C) = Kt$, where C_0 and C are the initial and actual concentration of RhB and K is the apparent rate constant of the degradation [31]. The degradation rate constants K of RhB were shown in Table 1 along with BET surface area of ZnO nanostructures. It can be seen that the maximum absorbance of 553 nm disappears almost completely after irradiation for about 8 h by suspension of ZnO nanodisks (Fig. 6a). Compared with the UV–vis spectra of the photocatalytic degradation of RhB by suspension of ZnO nanowires (Fig. 6b and c), the maximum absorbance of 553 nm still existed after irradiation for 8 h, indicating the incomplete photocatalytic degradation of the dye.

The incomplete photocatalytic degradations of RhB after 8 h were observed for thick and thin nanowires with different catalytic activities. The nanowires are all surrounded by absolute majority {01$\bar{1}$0} facets. The diameters of the nanowires are much larger than that of carrier recombination dynamics [20,32]. The latter is used to explain the optimized catalytic activity for nanocrystallines in several tens of nanometers. They posses distinctly different surface areas, which is 1.924, and 9.492 m^2/g (Table 1), respectively. We account the different photocatalytic activity of nanowires to their surface areas.

For the photocatalytic activity of ZnO nanostructures with different crystal planes, the specific surface area is not the most
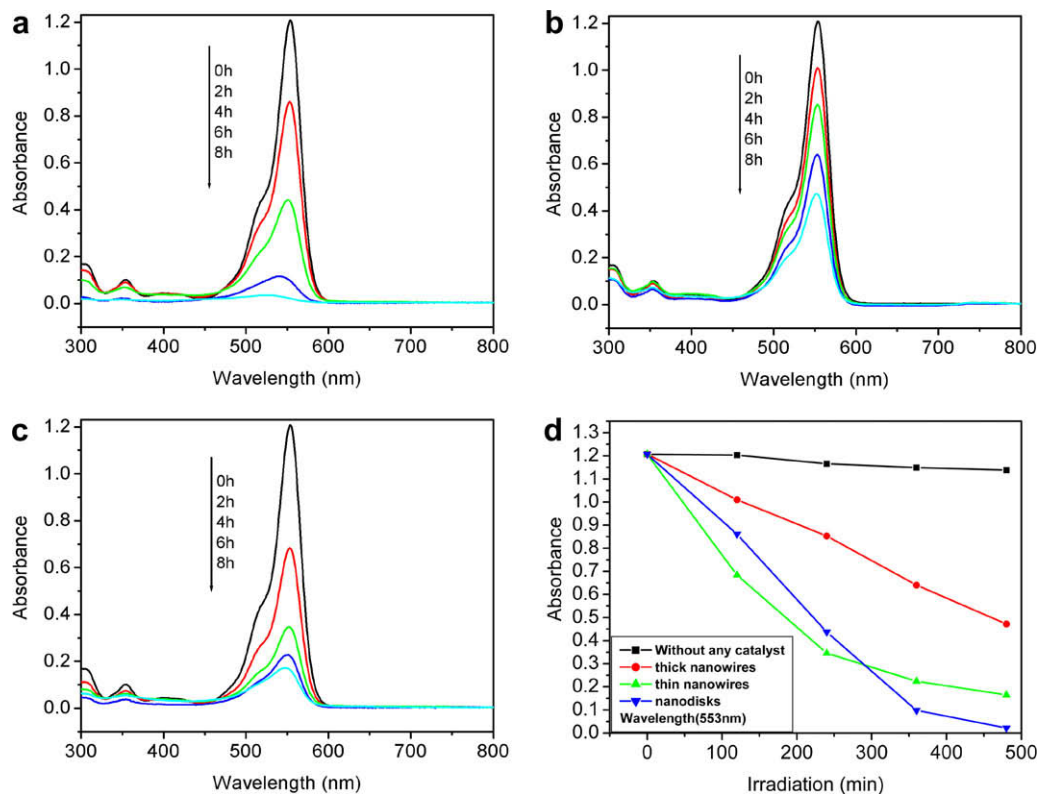
Fig. 6. Absorption spectra of Rhodamine B aqueous solution with different ZnO nanostructures after UV irradiation with different time. (a) ZnO nanodisks, (b) thick ZnO nanowires, (c) thin ZnO nanowires, (d) comparative studies of the photocatalytic activity of ZnO nanodisks and nanowires.

important factor and facets dominate the catalytic activity. An interesting phenomenon is revealed from the RhB degradation efficiency curve (Fig. 6d). Although the degradation efficiency of RhB for thin nanowire catalyst with a surface area of 9.492 m^2/g is the fastest among the three ZnO nanostructures in the initial 4 h, which is not beyond our expectation due to its largest surface area, the final degradation result of thin ZnO nanowires after 5 h illumination is much slower than ZnO nanodisks with even smaller surface area of 6.931 m^2/g. The low degradation rate of thin ZnO nanowires after 5 h may be related to the formation of some long-lived by-products covered on the surface of nanowire catalyst. These by-products are with low rate constants of reactions with hydroxyl radicals [33]. On the contrary, when the unique single-crystalline ZnO nanodisks are used as the catalyst, the maximum absorbance peak of RhB at 553 nm after UV irradiation for 8 h is 0.022 (Fig. 6a), much weaker than that for ZnO nanowires. More concrete data is that K_3 for ZnO nanodisk catalyst is significantly larger than K_1 and K_2, which clearly demonstrates that the nanodisks show superior photocatalytic activity over that of nanowires. SEM and HRTEM results have revealed that ZnO nanodisks predominantly expose polar {0001} planes, whereas in the ZnO nanowires nonpolar {01$\bar{1}$0} planes are the majority. This finding is an indication that ZnO nanodisks with well-defined reactive planes {0001} are more active than ZnO nanowires with the nonpolar {01$\bar{1}$0}.

However, the polar {0001} planes of ZnO possess both the Zn (0001) and O (000$\bar{1}$) planes with the same concentration. In terms of the previously proposed mechanism for the photocatalytic degradation of organic dye, we can clearly differentiate which plane was responsible for the photocatalytic activity. The conduction-band electrons (e_{cb}^-) and valence-band holes (h_{vb}^+) are generated on the surfaces of ZnO nanoparticles when ZnO nanostructures are illuminated by UV light with energy greater than the band gap energy. Holes can react with water adhering to the surfaces of ZnO nanostructures to form highly reactive hydroxyl radicals (OH·), while oxygen acts as an electron acceptor by forming a super-oxide radical anion (O_2^-). These super-oxide radical anions further form hydroxyl radicals, whose powerful oxidation ability can degrade organic dye [34]. ZnO crystal is a polar crystal, which can be described as a number of alternating planes composed of tetrahedrally coordinated O^{2-} and Zn^{2+} ions, stacked alternatively along the *c* axis. The oppositely charged ions produce positively charged Zn^{2+} (0001) and negatively charged O^{2-} (000$\bar{1}$) polar surfaces. Due to charge interaction, the negatively charged OH$^-$ were preferentially adsorbed on the positively charged Zn^{2+} (0001) surfaces of ZnO in an aqueous solution [24]. Then,

Table 1
BET surface area of ZnO nanostructures and degradation rate constants of RhB using nanodisks and nanowires as photocatalysts.

	Average diameter (μm)	Length or thickness (μm)	BET surface area (m^2/g)	Calculated area of ZnO (0001) face (m^2/g)	Apparent rate constant of the degradation ($K \times 10^{-3}$/min)	Ratio of rate constant
Thick nanowires	0.75	80	1.924	–	1.9561 (K_1)	–
Thin nanowires	0.2	100	9.492	–	4.1457 (K_2)	2.1194 (K_2/K_1)
Nanodisks	1.5	0.3	6.931	2.475	8.3434 (K_3)	4.2653 (K_3/K_1)

valence-band holes (h^+_{vb}) reacted with abundant OH^- adhering to the surfaces of ZnO (0001) planes to form highly reactive hydroxyl radicals ($OH^\cdot$) for degradation of organic dye. On the other hand, Zn (0001) plane holds the highest surface energy, and thus it is inherently more reactive than O ($000\bar{1}$) or nonpolar $\{01\bar{1}0\}$ can adsorb added organic dye to promote photocatalytic degradations of RhB. Because of charge interaction and the lower surface energy, O ($000\bar{1}$) and nonpolar $\{01\bar{1}0\}$ planes adsorb OH^- and organic dye are poorer than that of Zn (0001) plane, resulting in a lower activity. Compared with ZnO nanowires, ZnO nanodisks with a high (0001) facet population (2.475 m^2/g) and small surface area (Table 1) show the best photocatalytic activity. It is therefore concluded that the polar (0001) plane of ZnO is the most active site for photocatalytic RhB degradation.

4. Conclusion

Uniform single-crystalline ZnO nanodisks and nanowires with well-defined crystal planes have been synthesized hydrothermally. We also clearly demonstrated that the unique ZnO nanodisks with a high population of (0001) facet show better catalytic activity by the comparison of photodegradation of RhB with that of ZnO nanowires used as catalyst. The present results suggest that catalysts may be designed and synthesized to optimize the catalytic activity of nanocrystallnies with well-defined active facets.

References

[1] (a) N. Tian, Z.Y. Zhou, S.G. Sun, Y. Ding, Z.L. Wang, Science 316 (2007) 732;
(b) G.Y. Hua et al., Nature 453 (2008) 638.
[2] B.M. Choudary, R.S. Mulukutla, K.J. Klabunde, J. Am. Chem. Soc. 125 (2003) 2020.
[3] W. Chrzanowski, A. Wieckowski, Langmuir 14 (1998) 1967.
[4] (a) D.S. Sholl, A. Asthagiri, T.D. Power, J. Phys. Chem. B 105 (2001) 4771;
(b) T. Mallat, E. Orglmeister, A. Baiker, Chem. Rev. 107 (2007) 48663.
[5] (a) X.Q. Gong, A. Selloni, M. Batzill, U. Diebold, Nature Mater. 5 (2006) 665;
(b) U. Diebold, Surf. Sci. Rep. 48 (2003) 53;
(c) A.G. Thomas, Phys. Rev. B 67 (2003) 035110.
[6] (a) L. Kavan, M. Grätzel, S.E. Gilbert, C. Klemenz, H. Scheel, J. Am. Chem. Soc. 118 (1996) 6716;
(b) G.S. Herman, M.R. Sievers, Y. Gao, Phys. Rev. Lett. 84 (2000) 3354;
(c) M. Lazzeri, A. Selloni, Phys. Rev. Lett. 87 (2001) 266105.
[7] (a) R. Schlögl, S.B.A. Hamid, Angew. Chem., Int. Ed. 43 (2004) 1628;
(b) Y.J. Xiong, B.J. Wiley, Y.N. Xia, Angew. Chem., Intl. Ed. 46 (2007) 7157;
(c) A.R. Tao, S. Habas, P.D. Yang, Small 4 (2008) 310.
[8] Y.H. Zheng, L.R. Zheng, Y.Y. Zhan, X.Y. Lin, Q. Zheng, K.M. Wei, Inorg. Chem. 46 (2007) 6980.
[9] (a) V. Slack, G.A. Holliden, Sulfur Dioxide Removal from Waste Gases, second edn., Noyes Data Corporation, Park Ridge, NJ, 1975;
(b) C.N. Satterfield, Heterogeneous Catalysis in Practice, McGraw-Hill, New York, 1980, p. 261.
[10] M. Shimokawabe, A. Ohi, N. Takezawa, React. Kinet. Catal. Lett. 52 (1994) 393.
[11] S.A. French, A.A. Sokol, S.T. Bromley, C.R.A. Catlow, S.C. Rogers, F. King, P. Sherwood, Angew. Chem. 113 (2001) 4569.
[12] M.R. Hoffmann, E.R. Carraway, M.R. Hoffmann, Environ. Sci. Technol. 28 (1994) 776.
[13] C.H. Ye, Y. Bando, G.Z. Shen, D. Golberg, J. Phys. Chem. B 110 (2006) 15146.
[14] M.H. Huang et al., Science 292 (2001) 1897.
[15] (a) P. Gao, C. Ying, S.Q. Wang, L.N. Ye, Q.X. Guo, Y.J. Xie, Nanopar. Res. 8 (2006) 131;
(b) B.Q. Cao, W.P. Cai, Y. Li, F.Q. Sun, L.D. Zhang, Nanotechnology 16 (2005) 1734;
(c) F. Xu, Z.Y. Yuan, G.H. Du, M. Halasa, B.L. Su, Appl. Phys. A 86 (2007) 181;
(d) W.X. Zhang, K. Yanagisawa, Chem. Mater. 19 (2007) 2329;
(e) L.P. Bauermann, A. del Campo, J. Bill, F. Aldinger, Chem. Mater. 18 (2006) 2016;
(f) S.H. Jung, E. Oh, K.H. Lee, Y. Yang, C.G. Park, W. Park, S.H. Jeong, Cryst. Growth Des. 8 (2008) 265.
[16] (a) H. Zhang, D.R. Yang, D.S. Li, X.Y. Ma, S.Z. Li, D.L. Que, Cryst. Growth Des. 5 (2005) 517;
(b) H. Zhang, D.R. Yang, S.Z. Li, J.Y. Ma, Y.J. Ji, J. Xu, D.L. Que, Mater. Lett. 59 (2005) 1696.
[17] (a) Z.W. Pan, Z.R. Dai, Z.L. Wang, Science 291 (2001) 1947;
(b) X.Y. Kong, Z.L. Wang, Nano Lett. 3 (2003) 1625.
[18] (a) L. Guo, Y. Liang, H.B. Xu, P. Simon, Z.Y. Wu, J. Am. Chem. Soc. 124 (2002) 14864;
(b) B. Liu, H.C. Zeng, J. Am. Chem. Soc. 125 (2003) 4430.
[19] H.D. Yu, Z.P. Zhang, M.Y. Han, X.T. Hao, F.R. Zhu, J. Am. Chem. Soc. 127 (2005) 2378.
[20] J.Y. Lao, J.Y. Huang, D.Z. Wang, Z.F. Ren, Nano Lett. 3 (2003) 235.
[21] (a) Z.R. Tian, J.A. Voigt, J. Liu, B. Mckenzie, M.J. Mcdermott, J. Am. Chem. Soc. 124 (2002) 12954;
(b) Z.R. Tian et al., Nat. Mater. 2 (2003) 821;
(c) H.Q. Yan, R.R. He, J. Pham, P.D. Yang, Adv. Mater. 15 (2003) 402;
(d) Q. Wan, T.H. Wang, J.C. Zhao, Appl. Phys. Lett. 87 (2005) 083105.
[22] (a) J.Y. Lao, J.G. Wen, Z.F. Ren, Nano Lett. 2 (2002) 1287;
(b) B.H. Juárez, P.D. García, D. Golmayo, A. Blanco, C. López, Adv. Mater. 17 (2005) 2761;
(c) W.I. Park, D.H. Kim, S.W. Jung, G.C. Yi, Appl. Phys. Lett. 80 (2002) 4232;
(d) S.H. Jung, E. Oh, K.H. Lee, W. Park, S.H. Jeong, Adv. Mater. 19 (2007) 749.
[23] (a) D.W. Bahnemann, C. Kormann, M.R. Hoffmann, J. Phys. Chem. 91 (1987) 3789;
(b) A.C. Dodd, A.J. McKinley, M. Saunders, T.J. Tsuzuki, Nanopart. Res. 8 (2006) 43.
[24] E.S. Jang, J.H. Won, S.J. Hwang, J.H. Choy, Adv. Mater. 18 (2006) 3309.
[25] F. Lu, W.P. Cai, Y.G. Zhang, Adv. Func. Mater. 18 (2008) 1047.
[26] (a) J.A. Rodriguez, T. Jirsak, S. Chaturvedi, J. Dvorak, J. Mol. Catal. A 167 (2001) 47;
(b) A.W. Grant, J.H. Larsen, C.A. Perez, S. Lehto, M. Shmal, C.T. Campbell, J. Phys. Chem. B 105 (2001) 9273.
[27] H. Wilmer et al., Phys. Chem. Chem. Phys. 5 (2003) 4736.
[28] B.B. Jin, J.H. Zeng, Y.F. Wang, Q.Yang, submitted for publication.
[29] (a) S. Maensiria, P. Laokula, V. Promarak, J. Cryst. Growth 289 (2006) 102;
(b) H.X. Li, J.Y. Wang, H. Liu, C.H. Yang, H.Y. Xu, X. Li, H.M. Cui, Vacuum 77 (2004) 57.
[30] R. Alcántara, F.J. Fernández-Madrigal, C. Pérez-Vicente, J.L. Tirado, J.C. Jumas, Fourcade Olivier, J. Chem. Mater. 12 (2000) 3044.
[31] (a) T.J. Kuo, C.N. Lin, C.L. Kuo, M.H. Huang, Chem. Mater. 19 (2007) 514;
(b) F.H. Zhao et al., Chem. Mater. 20 (2008) 1197;
(c) L. Wang, L.X. Chang, B. Zhao, Z.Y. Yuan, G.S. Shao, W. Zheng, J. Inorg. Chem. 47 (2008) 1443.
[32] Z.B. Zhang, C.C. Wang, R. Zakaria, J.Y. Ying, J. Phys. Chem. B 102 (1998) 10871.
[33] (a) C. Wang, J.C. Zhao, X.M. Wang, B.X. Mai, G.Y. Sheng, P.A. Peng, J.M. Fu, Appl. Cat. B: Environ. 39 (2002) 269;
(b) C. Galindo, P. Jacques, A. Kalt, J. Photochem. Photobiol. A: Chem. 130 (2000) 35.
[34] M.R. Hoffmann, S.T. Martin, W. Choi, D.W. Bahnemann, Chem. Rev. 95 (1995) 69.